J. Fluid Mech. (2012), *vol.* 713, *pp.* 362–375. © Cambridge University Press 2012
doi:10.1017/jfm.2012.460

Exact solutions for wave propagation over a patch of large bottom corrugations

Jie Yu† and Guangfu Zheng

Department of Civil, Construction and Environmental Engineering, North Carolina State University, Raleigh, NC 27695-7908, USA

(Received 18 February 2012; revised 20 August 2012; accepted 16 September 2012; first published online 17 October 2012)

Applying the Floquet theory for linear motions (Howard & Yu, *J. Fluid Mech.*, vol. 593, 2007, pp. 209–234) to the problem of wave propagation over a patch of periodic bottom corrugations in an otherwise flat seabed, we show that exact solutions to this scattering problem can be constructed without any constraint on the bottom amplitude and/or slope. These solutions are able to describe both the slowly and fast varying aspects of the flow, in contrast to the analyses based on the general ideas of slowly varying waves. We use as an example the well-studied Bragg scattering by a patch of bottom corrugations to present some quantitative results and comparisons with experimental data.

Key words: coastal engineering, surface gravity waves, wave scattering

1. Introduction

In Howard & Yu (2007, hereafter referred to as HY07), a basis of exact solutions was developed for linearized irrotational time-periodic flow over a corrugated bottom of arbitrary amplitude. This was done using the idea of Floquet theory and a conformal transformation. The Floquet solutions in HY07 can be identified as analogues, for the periodic bottom, of the familiar propagating and evanescent waves over a flat bottom. As an illustration of the use of these solutions, HY07 also investigated the normal modes of a rectangular tank with a corrugated bottom. Yu & Howard (2010, hereafter referred to as YH10) provided some extensions to HY07, focusing on the solutions appropriate for higher-order Bragg resonances of water waves in analogy to the mth-order reflections in the original X-ray work, i.e. occurring when the water wavelength is $\sim 2/m$ times the bottom wavelength, where $m = 2, 3, \ldots$.

Whereas that previous example deals with flux conditions (Neumann boundary condition) at the lateral boundaries of a closed domain, in the present paper we explore the use of these Floquet solutions in a different class of boundary value problems in an open flow domain, i.e. the scattering of a wave train by a patch of bottom corrugations in an otherwise flat bed. Here, at the interfaces separating the regions with different beds, matching the normal derivative of the solution (flux) and solution itself (relating to pressure) are both required. This example also uses both the

† Email address for correspondence: jie_yu@ncsu.edu

https://doi.org/10.1017/jfm.2012.460 Published online by Cambridge University Press

flat-bottom and Floquet modes, demonstrating the analogy of the two on one hand and the difference on the other.

Problems of wave scattering by periodic topographies have been rather extensively studied in the literature, in particular following the work of Davies (1982) and Heathershaw (1982) on Bragg reflection when the water wavelength is close to twice the bottom wavelength. In various approximate methods, the assumption of small-amplitude bottom undulations is often made: e.g. Mei (1985), Kirby (1986), Hara & Mei (1987), Liu (1987), Nayfeh & Hawwa (1994), Liu & Yue (1998) and Yu & Mei (2000); see also Mei, Hara & Yu (2001) and references cited there. For large-amplitude bottom undulations, exact solutions are scarce even for linear motions, and numerical, or semi-numerical, methods have generally been sought, such as the boundary integral equation method (Dalrymple & Kirby 1986) and topography discretization method, in which the bottom is approximated into many horizontal steps and a series of flat-bottom linear wave propagation problems is then solved and matched at the interfaces between sections: e.g. Mattioli (1990, 1991), O'Hare & Davies (1992) and Rey (1992), among others. This latter technique is often used in modelling water waves over variable topographies, not necessarily spatially periodic: see the discussion in Athanassoulis & Belibassakis (1999) and references therein. While a very significant improvement of the method has been put forward in Athanassoulis & Belibassakis (1999) by including an additional sloping-bottom mode in the standard representation, this is still essentially a numerical method but much more efficient.

The application made here demonstrates that exact solutions can be obtained without any constraint on the bottom amplitude and/or slope, using the basis of Floquet solutions in HY07 and YH10. Furthermore, these solutions are able to describe both the slowly and fast varying aspects of the flow within the regime of linear theory. This contributes to the theoretical treatments of water wave propagation over variable topography, rather than to the explorations of new physics of water wave Bragg resonances.

In HY07 and YH10, the bottom corrugations were taken to be a family of a special form, parameterised amplitude. The main reason for such a choice is that the required conformal transformation is well known and, in particular, given by simple formulas. We continue with this special form here, but emphasize that it is not necessary, though for the purpose of the present example it provides considerable simplicity. Exact solutions can be obtained for a general periodic bottom of arbitrary waveform by a judicious construction of the required conformal map. This is explained in detail in Yu & Howard (2012).

This paper is structured as follows. To make the paper more self-contained, we briefly summarize in § 2 the Floquet solutions for linear motions on a corrugated bed of indefinite length. The nature of these solutions, their connection and analogy to the flat-bottom solutions are discussed. Formulation of wave propagation over a patch of bottom corrugations in an otherwise flat seabed is described in § 3, following the standard approach. We then apply this to the well-studied Bragg resonance problem in § 4, presenting some quantitative results and comparisons with experimental data. Concluding remarks follow in § 5.

2. Floquet theory for motions over bottom corrugations

Deferring details to HY07 and YH10, we here summarize the exact theory for linear motions on a periodic corrugated bottom of indefinite length. The bed profile, which

https://doi.org/10.1017/jfm.2012.460 Published online by Cambridge University Press

is approximately sinusoidal at small amplitude but increasingly cusp-like as amplitude increases, is given implicitly by

$$h_b(x) = \epsilon h \cos 2\xi, \quad \text{where } \xi - \epsilon k_B h \coth(2k_B h) \sin 2\xi = k_B x. \tag{2.1}$$

Here $k_B \equiv \pi/\lambda_{bar}$, with λ_{bar} being the bottom wavelength. Thus, h_b is π-periodic both in $k_B x$ and in ξ. Relative to the mean water depth h, the crest-to-trough height of the corrugations is 2ϵ. We do not assume ϵ to be small, but only require $\epsilon < \epsilon_*$, where $\epsilon_* = \tanh 2k_B h/(2k_B h)$, in order for (2.1) to be single-valued. Notice that the mean water depth averaged over x is $k_B h_0 = k_B h \left(1 + (1/2)\epsilon^2/\epsilon_*\right)$, which is greater than $k_B h$, the mean depth averaged over ξ. The difference is only significant for sufficiently large ϵ. For the scattering problem described in the next section, $k_B h$ is taken to be the water depth on the flat bed outside the corrugation patch.

For irrotational motions in the vertical plane (x, z), the velocity potential $\phi(x, z, t)$ is described by the Laplace equation, the linearized free surface boundary condition at $z = 0$ and vanishing normal velocity at the seabed $z = -h + h_b$. The conformal transformation,

$$k_B x = \xi - \epsilon b \sin 2\xi \cosh 2\eta, \quad k_B z = \eta - \epsilon b \cos 2\xi \sinh 2\eta, \tag{2.2}$$

where $b = k_B h/\sinh 2k_B h$, is used to map the corrugated bottom onto a flat bed $\eta = -k_B h$ and the undisturbed free surface $z = 0$ onto $\eta = 0$. For time-periodic motion of angular frequency ω, $\phi = \varphi(x, z)\mathrm{e}^{-\mathrm{i}\omega t} + \text{c.c.}$ In the mapped plane, the linearized problem can be solved exactly, obtaining the Floquet solutions as follows:

$$\varphi(\xi, \eta; \mu) = \mathrm{e}^{\mu\xi} \sum_{n=-\infty}^{\infty} D_n \mathrm{e}^{\mathrm{i}n\xi} \frac{\cosh\left[(n - \mathrm{i}\mu)\,(\eta + k_B h)\right]}{\cosh\left[(n - \mathrm{i}\mu)\,k_B h\right]}, \tag{2.3}$$

$$L_n D_n = D_{n-2} + D_{n+2}, \tag{2.4}$$

$$L_n = (\epsilon b)^{-1} \left\{1 - \lambda^{-1}\,(n - \mathrm{i}\mu) \tanh[(n - \mathrm{i}\mu)\,k_B h]\right\}, \tag{2.5}$$

where $\lambda = \omega^2 (g k_B)^{-1}$ is a dimensionless measure of frequency. Equation (2.3) represents a set of solutions, individually identified by the Floquet exponent (eigenvalue) μ. The Floquet exponent μ and the associated Fourier coefficients $D_n(\mu)$ are determined following the method in HY07 and YH10.

Given a frequency ω, one can find a set of Floquet solutions using (2.3)–(2.5), consisting of two wave modes, and two families of evanescent modes each of which has infinite numbers. For the wave modes, the spatial modulation of the wave amplitude can be exponential or oscillatory, corresponding to real or pure imaginary μ (and its negative) and depending on whether ω is inside or outside a resonance wedge (HY07, YH10). As $\epsilon \to 0$, the two wave modes approach standing waves on a flat bottom when the limiting frequency is a Bragg resonance frequency, or flat-bottom propagating waves otherwise. For the evanescent modes, the μ are real and approach the eigenvalues of the flat-bottom evanescent modes as $\epsilon \to 0$. The limiting behaviour indicates that this set of Floquet solutions is an analogue of the set of linear modes on a flat bottom for the given ω. The latter is known to form a complete basis for constructing solutions to various boundary value problems. This close analogy with the flat-bottom case suggests that these Floquet modes may be used in a similar manner in boundary value problems involving a corrugated bed. It is based on this hypothesis that the application in HY07 and YH10 was made, and will be made in § 3 for the scattering problem. A formal mathematical proof, that this is a complete set for periodic topographies, is yet to be provided.

https://doi.org/10.1017/jfm.2012.460 Published online by Cambridge University Press

Because of the very close analogy we use the same names for the 'propagating' and 'evanescent' Floquet solutions in the context of a corrugated bottom as for the ordinary propagating and evanescent waves over a flat bottom. However, one should not confuse one with the other because of the names. Both sets are exact solutions of the Laplace equation, but are exact linear water wave solutions only with the appropriate kind of bottom. In the topography discretization method mentioned in § 1, on each of the small horizontal bottom steps the solution is represented as a superposition of flat-bottom propagating and evanescent waves. Since the water depth on each step is slightly different, the evanescent waves are necessary in every section for matching the flow conditions at the interfaces. This seems to leave an impression that flat-bottom evanescent modes are in evidence over the whole domain – as indeed they are from the point of view of the topography discretization method. However, when there is a periodic wavy bottom, the flat-bottom modes, either propagating or evanescent, are not appropriate. What is appropriate are the exact Floquet solutions described above. They satisfy the boundary condition on the wavy bottom exactly. When the corrugated bed section comes to an end, by abutting a vertical wall (e.g. a tank with corrugated bottom, a wavemaker), or by meeting an adjacent section with a different kind of bed, it is necessary to satisfy the lateral boundary or matching conditions there. The complete solution is a superposition of both the 'propagating' and 'evanescent' Floquet solutions; the former are seen over the whole of the wavy-bottom section, while the latter are indeed 'evanescent' and make significant contribution only near the ends of the corrugated bed section.

3. Waves propagating over a patch of corrugations

Consider a patch of periodic corrugations (e.g. sandbars) on an otherwise flat seabed. Let the seabed be at $z = -h + h_b$, where

$$h_b = \begin{cases} 0 & -\infty < x < x_0, \\ h_b(x) & x_0 \leqslant x \leqslant x_1, \\ 0 & x_1 < x < \infty, \end{cases} \tag{3.1}$$

with $h_b(x)$ being given by (2.1). For the continuity of the seabed profile, we let $h_b(x) = 0$ at $x = x_0$ and $x = x_1$.

From the linear wave theory, the velocity potential $\phi(x, z, t)$ satisfies

$$\nabla^2\phi = 0 \quad \text{for} \quad -h + h_b \leqslant z \leqslant 0, \quad -\infty < x < \infty, \tag{3.2}$$

$$\phi_{tt} + g\phi_z = 0 \quad \text{at } z = 0, \tag{3.3}$$

$$\phi_z = \phi_x h_{b,x} \quad \text{at } z = -h + h_b. \tag{3.4}$$

We shall from here on use the dimensionless variables

$$(x', z') = k_B(x, z), \quad \phi' = (2\omega/gA_{in})\,\phi, \tag{3.5}$$

where A_{in} is the incident wave amplitude, and drop the primes for brevity. Given a frequency ω, $\phi = \varphi(x, z)\mathrm{e}^{-\mathrm{i}\omega t} + \text{c.c.}$ For the flat-bed regions,

$$\varphi = A^+\varphi_f^+ + A^-\varphi_f^- + \sum_{j=1,\infty} A_j^+\varphi_{fj}^+ \quad \text{for } x < x_0^-, \tag{3.6}$$

$$\varphi = B^+\varphi_f^+ + B^-\varphi_f^- + \sum_{j=1,\infty} B_j^-\varphi_{fj}^- \quad \text{for } x > x_1^+, \tag{3.7}$$

https://doi.org/10.1017/jfm.2012.460 Published online by Cambridge University Press

where

$$\varphi_f^{\pm} = -\mathrm{i}\frac{\cosh\mu^f(z+k_Bh)}{\cosh\mu^f k_Bh}\mathrm{e}^{\pm\mathrm{i}\mu^f x} \quad \text{and} \quad \varphi_{fj}^{\pm} = \frac{\cos\mu_j^f(z+k_Bh)}{\cos\mu_j^f k_Bh}\mathrm{e}^{\pm\mu_j^f x} \tag{3.8}$$

are, respectively, the flat-bottom propagating and evanescent modes (Mei 1989). Here $\mu^f = k/k_B$ and $\mu_j^f = \kappa_j/k_B$, satisfying the dispersion relationship

$$\omega^2 = gk\tanh(kh) = -g\kappa_j\tan\left(\kappa_j h\right), \quad j = 1, 2, \ldots. \tag{3.9}$$

Over the bottom corrugations,

$$\varphi = C^+\varphi_c^+ + C^-\varphi_c^- + \sum_{j=1,\infty}\left(C_j^+\varphi_{cj}^+ + C_j^-\varphi_{cj}^-\right) \quad \text{for } x_0^+ < x < x_1^-, \tag{3.10}$$

where $\varphi_c^{\pm}$ and $\varphi_{cj}^{\pm}$ are the Floquet solutions in § 2, corresponding to the wave modes with $\pm\mu^c$ and evanescent modes with $\pm\mu_j^c$ for the given incident frequency ω.

The coefficients A, B and C in (3.6), (3.7) and (3.10) are complex and determined following the usual procedure, i.e. by matching the flow field at the boundaries between the flat-bed and corrugated-bed regions. In the mapped plane, the images of the lateral boundaries $x = x_0$ and $x = x_1$ are, respectively, $\xi = \xi_0(\eta)$ and $\xi = \xi_1(\eta)$ for $-k_Bh \leqslant \eta \leqslant 0$, which are in general curves (HY07). A differential length $\mathrm{d}z$ at elevation z along the boundaries in the (x, z) plane is mapped onto an arclength $\mathrm{d}s$ at the corresponding elevation η along the appropriate curves. Let u_n be the normal velocity to the appropriate curves. We require the matching conditions for the normal velocity:

$$u|_{x=x_0^-} = [u_n\,\mathrm{d}s/\mathrm{d}z]_{\xi=\xi_0^+(\eta)}, \quad u|_{x=x_1^+} = [u_n\,\mathrm{d}s/\mathrm{d}z]_{\xi=\xi_1^-(\eta)} \quad \text{for all } z. \tag{3.11}$$

This ensures that the normal flux crossing an arbitrary differential length at any elevation is continuous, leading to the continuity of total flux cross the boundaries. The factor $\mathrm{d}s/\mathrm{d}z$ in (3.11) reflects the fact that conformal transformation preserves angles but not lengths. For the flat-bed regions, $u = \varphi_x$. On the corrugated-bed side,

$$u_n = \left(\varphi_\xi - \xi_{0,\eta}\varphi_\eta\right)\left(1+\xi_{0,\eta}^2\right)^{-1/2}, \tag{3.12}$$

$$\mathrm{d}s/\mathrm{d}z = (1 - 2\epsilon b\cosh 2\eta\cos 2\xi_0)^{-1}\left(1+\xi_{0,\eta}^2\right)^{-1/2} \tag{3.13}$$

at $\xi = \xi_0^+(\eta)$ and

$$u_n = \left(\varphi_\xi - \xi_{1,\eta}\varphi_\eta\right)\left(1+\xi_{1,\eta}^2\right)^{-1/2}, \tag{3.14}$$

$$\mathrm{d}s/\mathrm{d}z = (1 - 2\epsilon b\cosh 2\eta\cos 2\xi_1)^{-1}\left(1+\xi_{1,\eta}^2\right)^{-1/2} \tag{3.15}$$

at $\xi = \xi_1^-(\eta)$. The mapping between z and η is calculated using (2.2). Calculation of the curves $\xi = \xi_0(\eta)$ and $\xi = \xi_1(\eta)$ involves solving a Kepler equation. Details are referred to HY07.

From the linearized Bernoulli equation, $p = -\rho gz + \mathrm{i}\omega\rho\phi$ (dimensional form). Continuity of pressure then requires

$$\varphi|_{x=x_0^-} = \varphi|_{\xi=\xi_0^+(\eta)}, \quad \varphi|_{x=x_1^+} = \varphi|_{\xi=\xi_1^-(\eta)} \quad \text{for all } z. \tag{3.16}$$

The continuity of free surface $z = \zeta$ is a consequence of (3.16) at $z = 0$, following the linearized dynamic boundary condition on the free surface. Since $v = \varphi_z$, the continuity of the vertical velocity also follows. This is of course due to the linearity (and time-periodic solution) of the problem.

https://doi.org/10.1017/jfm.2012.460 Published online by Cambridge University Press

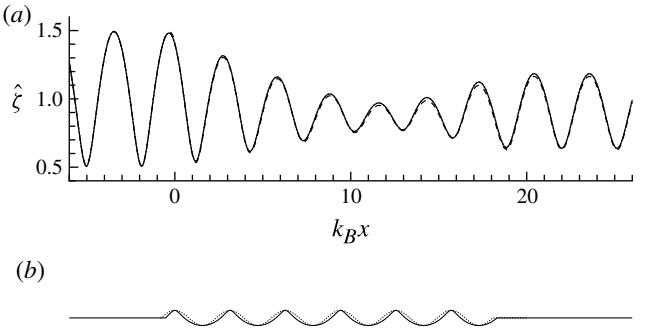


FIGURE 1. (*a*) Variation of surface amplitude $\hat{\zeta}(x)$ over a patch of corrugations, for $k_B h = 1.0$, $\omega/\omega_B = 1$, $\epsilon = 0.2410$, $N = 6$, $R_l = 0.3$, $\theta_l = \pi$. Lines: – – –, exact solution without evanescent modes; ——, exact solution with five evanescent modes; · · · · · ·, with ten evanescent modes (indistinguishable from that using five evanescent modes). (*b*) Bottom profile, in comparison with the simple sinusoidal form (dotted curve) of the same crest-to-trough height.

Let the incident wave train with frequency ω be arriving from $x \sim -\infty$. In (3.6), $A^+ = 1$ due to the normalization in (3.5). The effect of reflection from the shoreline, which is somewhere at $x > x_1$, can be simulated by imposing a complex reflection coefficient $R_l e^{i\theta_l}$ at $x = x_1^+$ (Yu & Mei 2000), which sets the ratio of oscillation amplitude of the left-going wave ($B^- e^{-i\mu^f x_1}$) to that of the right-going wave ($B^+ e^{+i\mu^f x_1}$), i.e.

$$R_l e^{i\theta_l} = \left(B^-/B^+\right) e^{-2i\mu^f x_1}. \tag{3.17}$$

Let the evanescent modes in (3.6), (3.7) and (3.10) be truncated at N_A, N_B and N_C, depending on the accuracy in satisfying the matching conditions at the lateral boundaries. Evaluating (3.11) and (3.16) at N_z discrete points of z, we obtain a linear system $QX = Y$, where vector X has a length $N_X = N_A + N_B + 2N_C + 4$ containing the coefficients A, B and C, and vector Y has a length N_z whose elements are either terms relating to A^+ or zeros. Matrix Q has dimensions $N_z \times N_X$. The least-squares solution to the system exists, as Q is column-independent. This least-squares solution gives the choice of coefficients A, B and C which minimize the errors to satisfy the conditions (3.11) and (3.16), constrained by the data points taken. The least-squares solution can be readily solved using mathematical software such as Maple or Matlab.

4. Application to water wave Bragg resonances

The formulation and solution in § 3 are applicable to waves of any frequency ω. For Bragg scattering of water waves, ω is close to $\omega_{Bm} \equiv g k_{Bm} \tanh(k_{Bm} h)$, where $k_{Bm} = m k_B$, $m = 1, 2, \ldots$, corresponding to wavelength $2\lambda_{bar}/m$. This phenomenon has been well studied in the literature and therefore provides a good example to illustrate the use of the exact solution in § 3. We have examined a number of cases, varying the water depth $k_B h$, wave frequency ω, corrugation amplitude ϵ and number N of corrugations in a patch. Some results are presented as follows.

Let the free surface be written as $\zeta(x, t) = \hat{\zeta}(x) \cos[\omega t + \alpha(x)]$, so $\hat{\zeta}(x)$ is the amplitude of surface oscillation at x. Figure 1 shows a sample graph of $\hat{\zeta}(x)$ varying

https://doi.org/10.1017/jfm.2012.460 Published online by Cambridge University Press

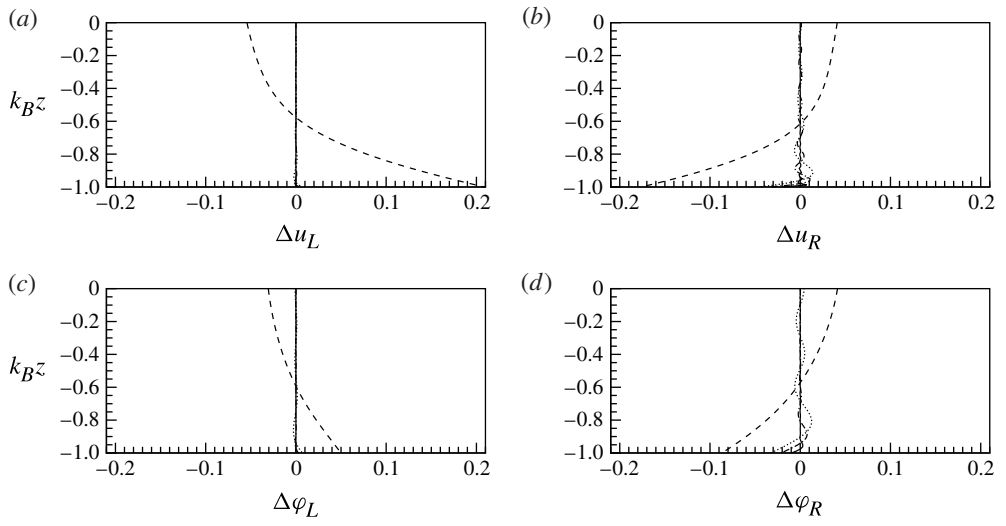


FIGURE 2. Accuracy in matching the lateral boundary conditions. Mismatch of normal velocity (*a*) at the incident end, $\Delta u_L = u|_{x_0^-} - [u_n\,\mathrm{d}s/\mathrm{d}z]_{\xi_0^+}$, (*b*) at the transmission end, $\Delta u_R = u|_{x_1^+} - [u_n\,\mathrm{d}s/\mathrm{d}z]_{\xi_1^-}$. Mismatch of pressure (i.e. velocity potential), (*c*) $\Delta\varphi_L = \varphi|_{x_0^-} - \varphi|_{\xi_0^+}$, (*d*) $\Delta\varphi_R = \varphi|_{x_1^+} - \varphi|_{\xi_1^-}$. Parameters are the same as in figure 1. Lines: – – –, exact solution without evanescent modes; · · · · · ·, exact solution with five evanescent modes; – · –, with ten evanescent modes; ——, with 40 evanescent modes.

over a patch of $N = 6$ bottom corrugations in water depth $k_Bh = 1.0$. With $\epsilon = 0.2410$ ($\epsilon/\epsilon_* = 0.5$), the crest-to-trough height of corrugations is ∼48 % of the water depth. Figure 1(*b*) shows the bottom profile in comparison with the simple sinusoidal form of the same crest-to-trough height. The incident wave frequency is $\omega = \omega_B$, i.e. tuned to the primary ($m = 1$) resonance. For the beach reflection, $R_l = 0.3$ and $\theta_l = \pi$. Five evanescent modes are included in the solution for each of the flat-bed regions, and five pairs ($\pm\mu_j^c$) in the solution for the corrugated-bed region. (The result using ten flat-bed modes and ten pairs of Floquet modes is also included, but it is hardly distinguishable from that using half the number of the appropriate modes.) As expected, $\hat{\zeta}(x)$ varies exponentially over the corrugation patch, decreasing then increasing onshore (The individual Floquet solutions vary exponentially, but the full solution is more like a hyperbolic cosine.) At the transmission end of the patch, the surface amplitude is ∼65 % of that at the incident end. Approximate theories (e.g. Mei 1985; Kirby 1986; Yu & Mei 2000) often focus on the slow modulation of surface amplitude and neglect the fast varying aspects of the motion that are usually confined to the regions close to lateral boundaries. These fast motions are resolved by the evanescent modes. In figure 1, we have included the result of $\hat{\zeta}(x)$ by deliberately omitting the evanescent modes from the solution. Even though this has an insignificant effect on $\hat{\zeta}(x)$, it is seen from figure 2 that the mismatch in lateral boundary conditions can be 20 % due to the omission of evanescent modes. This is consistent with the results in HY07 and YH10 that evanescent modes are important to the vertical structure of the flow close to lateral boundaries, having in general weaker effects on the surface profiles. In figure 2, results using more evanescent modes are included to show the increase of accuracy in satisfying the matching conditions (3.11) and (3.16). We must, however, remind readers that the number of evanescent modes used here is simply an issue of truncating

https://doi.org/10.1017/jfm.2012.460 Published online by Cambridge University Press

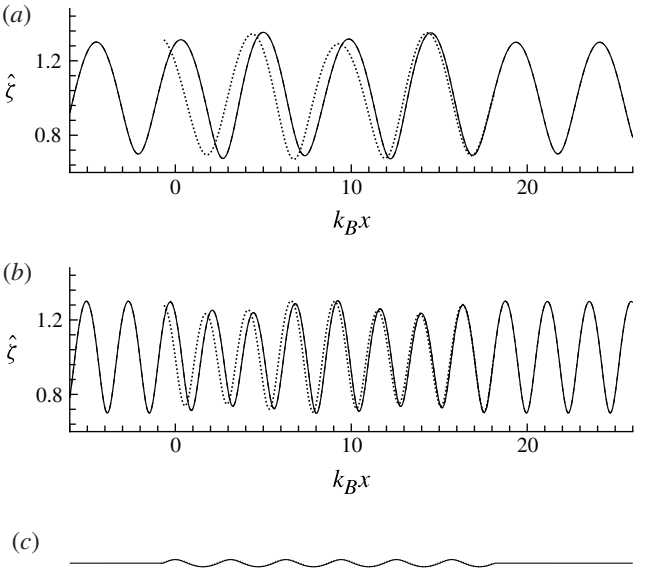


FIGURE 3. Variation of surface amplitude for detuned waves: (*a*) $\omega/\omega_B = 0.7072$; (*b*) $\omega/\omega_B = 1.2247$. Parameters: $k_B h = 1.0$, $\epsilon = 0.1$, $N = 6$, $R_l = 0.3$, $\theta_l = \pi/2$. Lines: ——, exact solution with evanescent modes; ·····, asymptotic theory (Yu & Mei 2000). (*c*) Bottom profiles. For the asymptotic theory, $h_b = \epsilon h \cos 2x$ and $\epsilon = 0.1$ (dotted curve).

a series giving the exact solution. It has little relation to the number of flat-bottom evanescent modes used in the piecewise bed approaches. There, the flat-bottom modes are used on every segment of the discretizations to locally approximate the solution. The number of those flat-bottom modes used is therefore an issue of the convergence of such an approximation, and in general increases as the bed becomes more rapidly varying. (Correspondingly refined discretization is also often needed.)

From various examples, it is observed that the influence of evanescent modes generally becomes stronger when we increase the water depth $k_B h$ and corrugation amplitude ϵ. This is expected. The beach reflection R_l does not significantly influence the matching of lateral boundary conditions. However, given a value of R_l, the mismatch is generally least when $\theta_l = \pi/2$, i.e. when the surface at the transmission end $x = x_1$ is midway between a surface envelope maximum ($\theta_l = 0$) and a minimum ($\theta_l = \pi$). It is also observed that in some cases $\hat{\zeta}(x)$ can be noticeably affected by the omission of evanescent modes; for instance, for $k_B h = 1.0$, $\epsilon = 0.2410$, $N = 6$, $R_l = 1.0$ and $\theta_l = \pi$, $\hat{\zeta}(x)$ can be underestimated by 15 % throughout.

The asymptotic theory in Mei (1985) has been used for comparisons in various experimental and numerical studies. Its extension to include the effects of shoreline reflection is given in Yu & Mei (2000). It is found that in most cases the asymptotic theory gives an accurate prediction of $\hat{\zeta}(x)$, compared with the exact solution, but only satisfies the lateral boundary conditions with fairly low accuracy as it does not include the evanescent modes. This is in general consistent with the results in HY07. However, significant discrepancy in $\hat{\zeta}(x)$ can be observed even for small ϵ, in particular when the waves are detuned away from the resonance frequency ω_B (see figure 3), and in cases where exponential onshore increase of $\hat{\zeta}(x)$ occurs (see figure 4). The wave frequencies in figure 3 are $\omega/\omega_B = 0.7072$ and $\omega/\omega_B = 1.2247$, just outside the

https://doi.org/10.1017/jfm.2012.460 Published online by Cambridge University Press

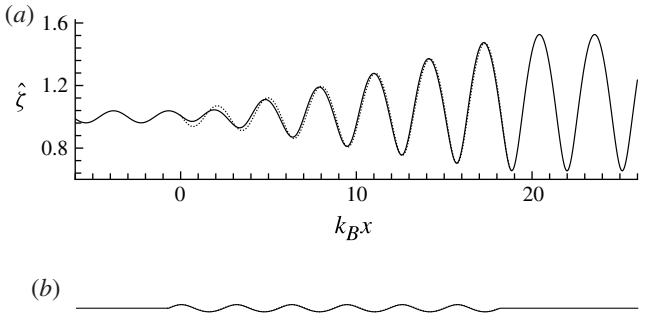


FIGURE 4. Graphs of $\hat{\zeta}(x)$ for $k_B h = 0.5$, $\omega/\omega_B = 1$, $N = 6$, $\epsilon = 0.1$, $R_l = 0.4$ and $\theta_l = \pi$. Lines: ——, exact solution with evanescent modes; ·····, asymptotic theory (Yu & Mei 2000). (*b*) Bottom profiles. For the asymptotic theory, $h_b = \epsilon h \cos 2x$ and $\epsilon = 0.1$ (dotted curve).

resonance wedge ($0.9864 < \omega/\omega_B < 1.0139$) for exponential modulation. It is seen that the scattered wave given by the asymptotic theory has a longer wavelength over the corrugation patch, becoming increasingly out of phase with the exact solution as we move seaward. The discrepancy is expected as the asymptotic theory assumes the wave frequency to be close to ω_B.

Sample graphs of $\hat{\zeta}(x)$ in cases of higher-order ($m > 1$) Bragg resonances are shown in figure 5, for $N = 6$ and $\epsilon = 0.4$. The incident wavelength is taken to be $k = mk_B$ such that the incident wave frequency is $\omega = \omega_{Bm}$. The water depth is fixed at $k_B h = 0.5$ in all cases. As m increases, the incident wave becomes shorter and less affected by the bottom topography. Still, significant effects can be seen even for $m = 3$ where $kh = 1.5$. For sufficiently large beach reflection, monotonic onshore increase of $\hat{\zeta}(x)$ can be obtained by varying the parameters: see figure 5(*b*). For $m = 4$, ω_{B4} is outside the resonance tongue (YH10), and the amplitude modulation is oscillatory. However, the oscillation period can be so long that the variation of $\hat{\zeta}(x)$ appears to be monotonic over the patch of six corrugations: see figure 5(*d*). In addition to the long-range exponential modulation due to Bragg resonances, it is seen that for $m = 2$ a higher peak (surface envelope maximum) is followed by a lower peak, for $m = 3$ two higher peaks are followed by a lower one, and for $m = 4$ two higher ones are followed by two lower ones. The period of these short-range modulations is one corrugation wavelength. The short-range modulations have similarly been observed for the normal modes of a tank with a corrugated bottom (YH10).

A comprehensive laboratory study of water wave Bragg resonance ($m = 1$) was reported in Davies & Heathershaw (1984) for a sinusoidal bottom. These experiments have been extensively used in the literature for comparison: e.g. Davies & Heathershaw (1984), Mei (1985), Dalrymple & Kirby (1986) and Kirby (1986), among others. Details of experimental setup and measurements were documented in Davies & Heathershaw (1983). In figure 6, we compare the measured and predicted $R(x)$ over a patch of $N = 10$ corrugations for $\epsilon = 0.16$, 0.18 and 0.2. In figure 7, the spatial variations of $\hat{\zeta}(x)$ and $-\hat{\zeta}(x)$ are plotted for the same cases, compared with the data. The incident wave arrives from $x < 0$. The non-zero R_l, due to reflection from the beach, is determined from the measurements for $x > x_1$. The phase angle θ_l cannot be obtained from the data. We have carried out the calculations varying θ_l from 0 to π, and found no significant differences. The results presented here are for $\theta_l = \pi/2$. For

https://doi.org/10.1017/jfm.2012.460 Published online by Cambridge University Press

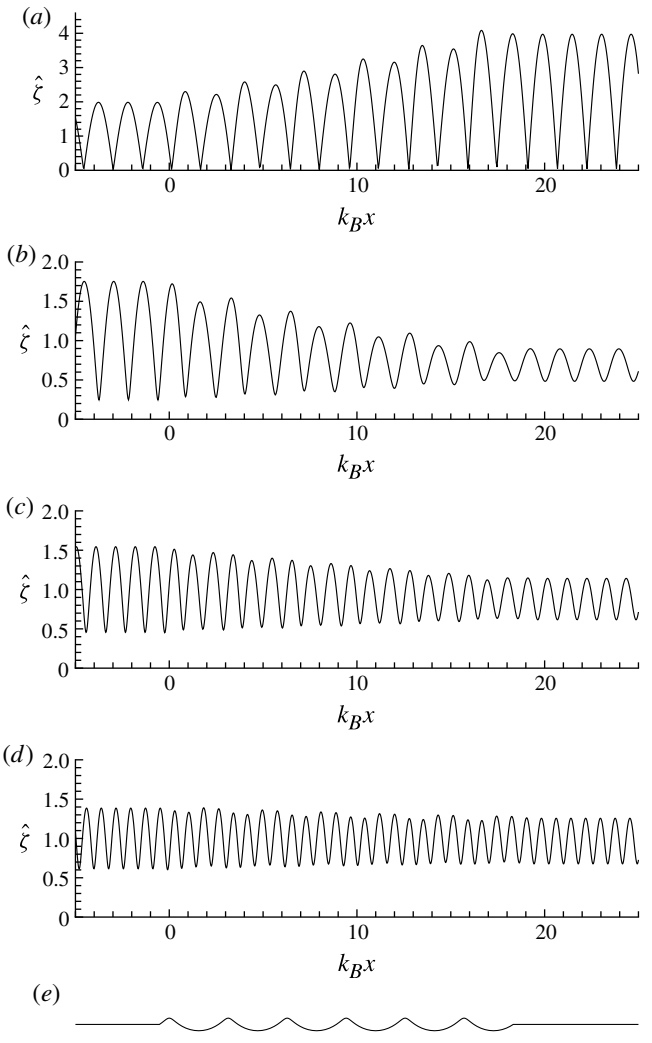


FIGURE 5. Surface amplitude $\hat{\zeta}(x)$ in cases of higher-order Bragg resonances, for $k_B h = 0.5$, $N = 6$, $\epsilon = 0.4$: (*a*) $m = 1$, $k = 2k_B$, $\omega/\omega_B = 1$, $R_l = 1.0$, $\theta_l = 3\pi/4$; (*b*) $m = 2$, $k = 2k_B$, $\omega/\omega_{B2} = 1$, $R_l = 0.3$, $\theta_l = \pi/2$; (*c*) $m = 3$, $k = 3k_B$, $\omega/\omega_{B3} = 1$, $R_l = 0.3$, $\theta_l = \pi/2$; (*d*) $m = 4$, $k = 4k_B$, $\omega/\omega_{B4} = 1$, $R_l = 0.3$, $\theta_l = \pi/2$.

the Floquet solutions, $R(x)$ is determined using the dominant terms of the reflected and incident waves, i.e.

$$R(x) = \left| \frac{C^+ \mathrm{e}^{\mu^c \xi} D_{-1}(\mu^c) + C^- \mathrm{e}^{-\mu^c \xi} D_{-1}(-\mu^c)}{C^+ \mathrm{e}^{\mu^c \xi} D_1(\mu^c) + C^- \mathrm{e}^{-\mu^c \xi} D_1(-\mu^c)} \right| \quad \text{for } x_0 < x < x_1, \tag{4.1}$$

consistent with the method in Goda & Suzuki (1977) which was used in the experiments. For the flat-bed regions,

$$R = |A^-| \quad \text{for } x < x_0, \quad R = |B^-/B^+| \quad \text{for } x > x_1. \tag{4.2}$$

The exact solution gives very good predictions of $R(x)$ over the corrugations. On the incident side of the patch for $x < 0$, the data show a decrease in $R(x)$ as we

https://doi.org/10.1017/jfm.2012.460 Published online by Cambridge University Press

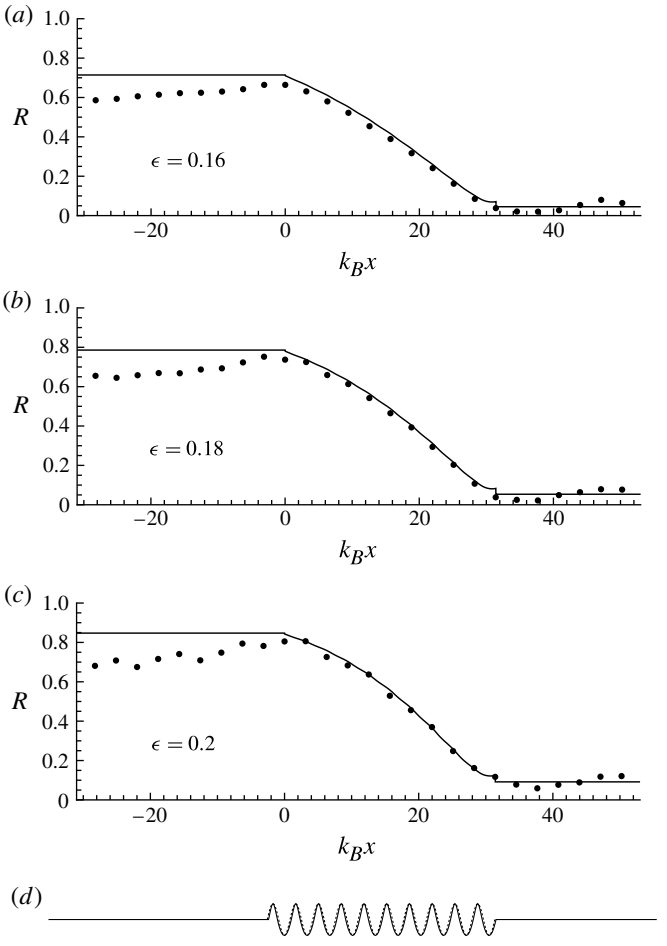


FIGURE 6. Spatial variation of reflection coefficient $R(x)$ over the corrugation patch and outside it: (*a*) $k_Bh = 0.9833$, $\omega/\omega_B = 0.9944$, $R_l = 0.045$, $\theta_l = \pi/2$; (*b*) $k_Bh = 0.8734$, $\omega/\omega_B = 0.9850$, $R_l = 0.054$, $\theta_l = \pi/2$; (*c*) $k_Bh = 0.7854$, $\omega/\omega_B = 0.9842$, $R_l = 0.092$, $\theta_l = \pi/2$. •, data (Davies & Heathershaw 1984); ——, exact theory. (*d*) Bottom profiles for $\epsilon = 0.2$ and $k_Bh = 0.7854$. The simple sinusoidal profile is shown in the dotted curve.

move toward the wavemaker. For linear waves on a flat bed, $R(x)$ is constant. Davies & Heathershaw (1983, 1984) remarked that this decrease in $R(x)$ could be due to the viscous dissipation, as well as reflections from the wavemaker. There are also small discrepancies on the transmission side of the patch due to the variations in the data. While the measurements $\hat{\zeta}(x)$ agree fairly well with the theory, they deviate from the perfect $\pm$ symmetry of the theoretical curves, in particular for large ϵ; the measured $-\hat{\zeta}(x)$ are generally smaller in magnitude. The asymmetry in the data was not explained. Some possible explanations can be nonlinearities in the flow, or surface tension effects on the wires of wave gauges.

The reflection coefficient R_{up} for $x < 0$ may be used to measure the total effect of the corrugation patch due to Bragg scattering. Figure 8(*a*,*b*) shows R_{up} as a function of k/k_B for $N = 10$ and $N = 4$. The overall agreement is good. The exact solution with non-zero R_l (taken from the measurements) shows better agreement with the data

https://doi.org/10.1017/jfm.2012.460 Published online by Cambridge University Press

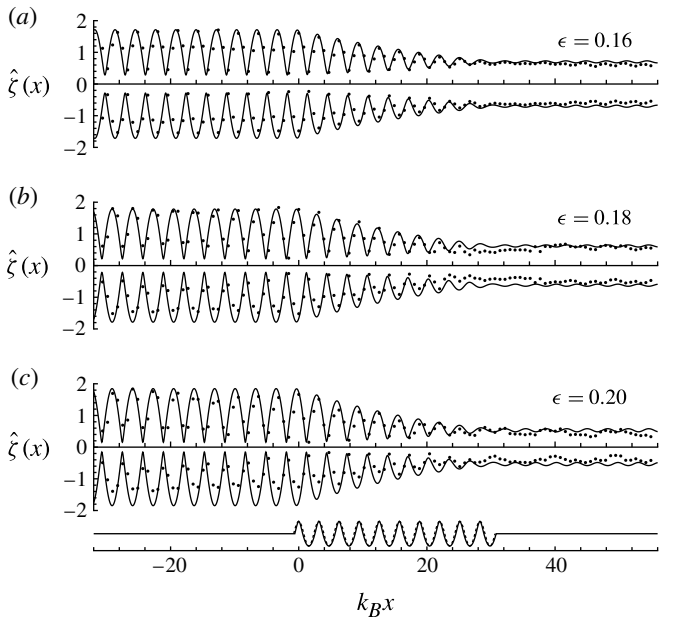


FIGURE 7. Spatial variations of surface amplitude over the corrugation patch and outside it. The measurements are normalized by the incident wave amplitude: $A_{in} = 1.06$ cm in (*a*), $A_{in} = 2.42$ cm in (*b*), and $A_{in} = 2.24$ cm in (*c*). Parameters are the same as in figure 6 for the corresponding cases. •, data (Davies & Heathershaw 1984); ——, exact theory.

for $k/k_B < 1$ than the prediction using $R_l = 0$. In both cases, the exact theory gives a smaller second peak at $k/k_B = 2$ due to the second-order $m = 2$ Bragg resonance. This is not indicated by the data, but has been previously observed in numerical studies (Mattioli 1990, 1991; O'Hare & Davies 1992). One possible explanation for the discrepancy could be the more cusp-shaped corrugations used in the exact solutions, versus the pure sinusoidal bed in the experiments, as the $m > 1$ resonance tongues can be quite varied and complex depending on the bed forms (Yu & Howard 2012). On the other hand, more precise wave measurement and control may be needed in order to capture those higher-order resonance peaks, which tend to be small and narrow.

5. Concluding remarks

We have shown how to construct exact solutions for linear waves propagating over a patch of bottom corrugations in an otherwise flat seabed, without any constraint on the bottom amplitude or slope, by using the basis of Floquet solutions developed in HY07 and YH10. These solutions give the descriptions of both the slowly and fast varying aspects of the flow, in contrast to the theories based on the general ideas of slowly varying waves. We have applied them to the problem of Bragg scattering of water waves by a patch of periodic bottom, compared with the existing experiments and approximate theory, both of which are well cited in the literature.

The solution method developed is not restricted to the special form of the bottom corrugations, which is chosen for mathematical simplicity. It can be readily applied to the study of wave scattering by a general periodic topography of arbitrary amplitude and shape, using the basis of exact solutions provided in Yu & Howard (2012). Linear

https://doi.org/10.1017/jfm.2012.460 Published online by Cambridge University Press

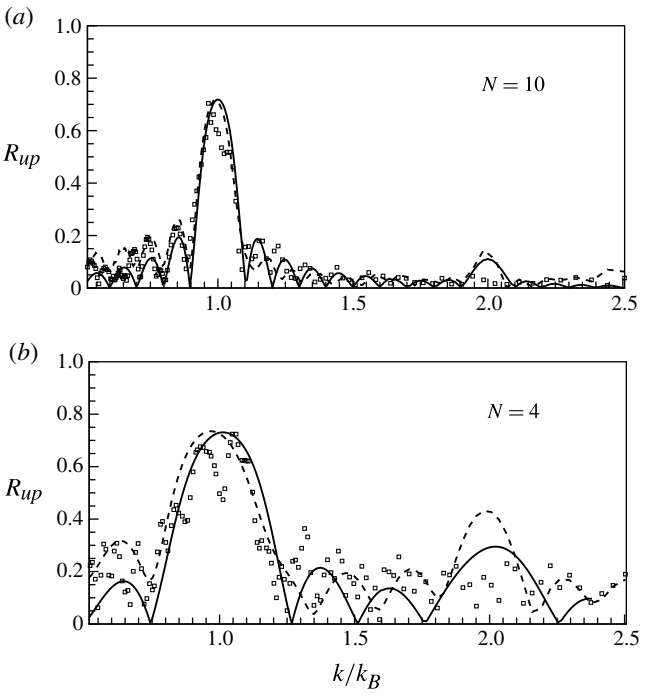


FIGURE 8. Reflection coefficient R_{up} on the incident side of the corrugation patch as a function of k/k_B: (*a*) $\epsilon = 0.16$ and $h = 31.3$ cm; (*b*) $\epsilon = 0.32$ and $h = 15.6$ cm. □, data (Davies & Heathershaw 1984); – – –, exact theory ($R_l \neq 0$); ——, exact theory ($R_l = 0$). In (*a*) R_l is taken from the measurements at each data point k/k_B, but in (*b*) R_l is set to be the average over the measurements for $x > x_1$ due to the scatter in data.

solutions are often applied in engineering applications to provide useful information. Nonlinear analyses typically begin with linear solutions. In view of the fact that even for linear motions over a simple regular periodic bottom there have been few exact solutions, and that numerical methods can be costly when the bottom amplitude (and/or slope) is large, the contribution of these exact solutions to the theoretical treatments of water wave propagation over periodic topographies in general, need not be particularly stressed.

Acknowledgement

Support by US National Science Foundation (Grants CBET-0756271 and CBET-0845957) is gratefully acknowledged.

REFERENCES

ATHANASSOULIS, G. A. & BELIBASSAKIS, K. A. 1999 A consistent coupled-mode theory for the propagation of small-amplitude water waves over variable bathymetry regions. *J. Fluid Mech.* **389**, 275–301.

DALRYMPLE, R. A. & KIRBY, J. T. 1986 Water waves over ripples. *J. Waterways Port Coast. Ocean Engng* **112**, 309–319.

DAVIES, A. G. 1982 The reflection of wave energy by undulations on the seabed. *Dyn. Atmos. Oceans* **6**, 207–232.

https://doi.org/10.1017/jfm.2012.460 Published online by Cambridge University Press

DAVIES, A. G. & HEATHERSHAW, A. D. 1983 Surface wave propagation over sinusoidally varying topography: theory and observation. Institute of Oceanographic Sciences report 159.

DAVIES, A. G. & HEATHERSHAW, A. D. 1984 Surface wave propagation over sinusoidally varying topography. *J. Fluid Mech.* **144**, 419–443.

GODA, Y & SUZUKI, Y. 1977 Estimation of incident and reflected waves in random wave experiments. In *Proc. 15th Intl Conf. on Coastal Engng, 1976*, pp. 828–845. ASCE.

HARA, T. & MEI, C. C. 1987 Bragg scattering of surface waves by periodic bars: theory and experiment. *J. Fluid Mech.* **178**, 221–241.

HEATHERSHAW, A. D. 1982 Seabed-wave resonance and sand bar growth. *Nature* **296**, 343–345.

HOWARD, L. N. & YU, J. 2007 Normal modes of a rectangular tank with corrugated bottom. *J. Fluid Mech.* **593**, 209–234.

KIRBY, J. T. 1986 A general wave equation for waves over rippled beds. *J. Fluid Mech.* **162**, 171–186.

LIU, P. L.-F. 1987 Resonant reflection of water waves in a long channel with corrugated boundaries. *J. Fluid Mech.* **179**, 371–381.

LIU, Y. & YUE, D. K. P. 1998 On generalized Bragg scattering of surface waves by bottom ripples. *J. Fluid Mech.* **356**, 297–326.

MATTIOLI, F. 1990 Resonance reflection of a series of submerged breakwaters. *Il Nuovo Cimento* C **13**, 823–833.

MATTIOLI, F. 1991 Resonance reflection of surface waves by non-sinusoidal bottom undulations. *Appl. Ocean Res.* **13**, 49–53.

MEI, C. C. 1985 Resonant reflection of surface water waves by periodic sandbars. *J. Fluid Mech.* **152**, 315–337.

MEI, C. C. 1989 *The Applied Dynamics of Ocean Surface Waves*. World Scientific.

MEI, C. C., HARA, T. & YU, J. 2001 Longshore bars and Bragg resonance. In *Geomorphological Fluid Mechanics* (ed. N. Balmforth & A. Provenzale), *Lecture Notes in Physics*, vol. 582, chap. 20, pp. 500–527. Springer.

NAYFEH, A. H. & HAWWA, M. A. 1994 Interaction of surface gravity waves on a non-uniformly periodic seabed. *Phys. Fluids* **6**, 209–213.

O'HARE, T. J. & DAVIES, A. G. 1992 A new model for surface wave propagation over undulating topography. *Coast. Engng* **18**, 251–266.

REY, V. 1992 Propagation and local behavior of normal incident gravity waves over varying topographies. *Eur. J. Mech.* B **11**, 213–232.

YU, J. & HOWARD, L. N. 2010 On higher order Bragg resonance of water waves by bottom corrugations. *J. Fluid Mech.* **659**, 484–504.

YU, J. & HOWARD, L. N. 2012 Exact Floquet theory for waves over arbitrary periodic topographies. *J. Fluid Mech.* **712**, 451–470.

YU, J. & MEI, C. C. 2000 Do longshore bars shelter the shore? *J. Fluid Mech.* **404**, 251–268.

https://doi.org/10.1017/jfm.2012.460 Published online by Cambridge University Press